

Impact of electron spectra on morphology of pulsar halos at ultra-high energies

Ying-Ying Guo^a, Qiang Yuan^{a,b,*}

^aKey Laboratory of Dark Matter and Space Astronomy, Purple Mountain Observatory, Chinese Academy of Sciences, Nanjing 210023, China

^bSchool of Astronomy and Space Science, University of Science and Technology of China, Hefei 230026, China

Abstract

The extended γ -ray halos around pulsars are unique probe of transportation of high-energy electrons (and positrons) in vicinities of such pulsars. Observations of morphologies of several such halos indicate that particles diffuse very slowly around pulsars, compared with that in the Milky Way halo. The energy-dependent morphologies are expected to be very important in studying the energy-dependence of the diffusion coefficient. In this work we point out that the spectrum of high-energy electrons takes effect in shaping the γ -ray morphologies at the ultra-high-energy bands, and thus results in a degeneracy between the electron spectrum and the energy-dependence of the diffusion coefficient. The reasons for such a degeneracy include both the Klein-Nishina effect of the inverse Compton scattering and the curvature (if any) of the electron spectrum. It is thus necessary to take into account the spectral shape of electrons when deriving the energy-dependence of diffusion coefficient using ultra-high-energy γ -ray measurements of extended pulsar halos.

Keywords: pulsar halos, diffusion propagation, energy losses

1. Introduction

Charged cosmic rays (CRs) are expected to propagate diffusively in the interstellar medium (ISM) due to scattering with random magnetized turbulence [1, 2]. According to the resonant scattering theory between particles and the interstellar turbulence, the rigidity-dependence of the diffusion coefficient follows a power-law, $D(R) \propto R^\delta$, given a power-law form of the spectral energy density of turbulence, $w(k) \propto k^{-2+\delta}$ where k is the wave number of the magnetohydrodynamic waves. Fitting to the CR secondary-to-primary ratios, the parameter δ is found to be about 0.3 – 0.6 for energies below TeV/n [3, 4]. Further precise measurements of the secondary-to-primary ratios show that there are hardenings of such ratios at high energies [5, 6], suggesting possible changes of the slope of rigidity-dependence of the diffusion coefficient [7].

The secondary-to-primary ratios reflect an average effect of the propagation of CRs in the Milky Way. It is very likely that the propagation is spatially dependent. Such a scenario was proposed to explain some observational results of CRs and diffuse γ rays [8, 9, 10, 11]. Observations of extended γ -ray halos surrounding middle-aged pulsars, which are expected to be produced by the inverse Compton scattering (ICS) of high energy electrons (and positrons) produced by the pulsars with the interstellar radiation field, offer a more direct measurement of the particle diffusion in specific regions of the ISM [12, 13]. The results show that electrons propagate much more slowly around pulsars than that in the Milky Way halo, indicating an inhomogeneous propagation of particles [14, 15]. Additional supports

for an inhomogeneous propagation were also given from the spectra of electrons and positrons, nuclei, and the large-scale anisotropies [16, 17, 18].

Detailed morphological studies of the γ -ray pulsar halos are very important in measuring the energy-dependence of diffusion coefficient, and testing its generality in different places of the Milky Way. Due to the fast energy losses of electrons in the ISM (synchrotron losses and the ICS losses), higher energy electrons experience shorter lifetime which approximately scales as $\tau(E_e) \propto E_e^{-1}$. Depending on the slope δ of the diffusion coefficient, the extensions of γ -ray halos may increase (for $\delta > 1$) or shrink (for $\delta < 1$) when energy increases. This expectation does not rely on the spectrum of electrons, and may hold for specific energy range where the cooling dominates the diffusion, the ICS lies well in the Thomson regime and the electron spectrum follows roughly a power-law. However, in the ultra-high-energy (UHE) range (with γ -ray energy E_γ higher than tens of TeV) many of the above assumptions are invalid, and this simple expectation should not hold any more [19]. In this work, we study the energy-dependent morphologies of pulsar halos in the UHE range assuming different spectral shapes. We will show that the electron spectrum couples with the diffusion process to shape the γ -ray morphologies and complicates the measurement of the energy-dependence of the diffusion coefficient. This effect cannot be ignored since at UHE spectral cutoff is common for source acceleration.

*Corresponding author

Email address: yuanq@pmo.ac.cn (Qiang Yuan)

2. Injection and propagation of electrons from pulsars

The propagation of electrons (and positrons) in the ISM around a pulsar is described by the diffusion-cooling equation

$$\frac{\partial N}{\partial t} = \nabla \cdot (D \nabla N) + \frac{\partial}{\partial E_e} (bN) + Q, \quad (1)$$

where E_e is the energy of electrons, $N = N(r, E_e, t)$ is the differential density of electrons, $D = D(E_e)$ is the diffusion coefficient, $b = b(E_e) = -dE_e/dt$ is the energy loss rate, and $Q = Q(r, E_e, t)$ represents the source term. In this work we focus on electron propagation near the pulsar, and neglect possible spatial variations of the diffusion coefficient and the energy loss rate.

The diffusion coefficient is parameterized as a power-law of electron energy, $D(E_e) = D_0 E_e^\delta$. The cooling of electrons includes mainly the synchrotron cooling and ICS cooling. The energy loss rate of synchrotron radiation is

$$b_{\text{syn}}(E_e) = \frac{4}{3} \sigma_T c \gamma_e^2 U_B, \quad (2)$$

where σ_T is the Thomson cross section, $\gamma_e = E_e/(m_e c^2)$ is the Lorentz factor of electron, m_e is the electron mass, c is the speed of light, and $U_B = B^2/(8\pi)$ is the energy density of the magnetic field with strength B . In this work, $B = 3 \mu\text{G}$ is assumed¹. For the cooling rate due to the ICS emission, we use the approximation given in Ref. [20]. We assume three gray (black) body components of the interstellar radiation fields (ISRF), the cosmic microwave background with temperature of 2.725 K and energy density of 0.26 eV cm^{-3} , an infrared background with temperature of 20 K and energy density of 0.3 eV cm^{-3} , and an optical component with temperature of 5000 K and energy density of 0.3 eV cm^{-3} , respectively.

The injection function is assumed to be a point source in space, a power-law with (super)-exponential cutoff in energy, and a profile following the pulsar spindown in time:

$$Q(\mathbf{r}, E_e, t) = Q_0 \delta(\mathbf{r} - \mathbf{r}_{\text{psr}}) \times E_e^{-\alpha} \exp[-(E_e/E_c)^\beta] \times (1 + t/\tau_0)^{-2}, \quad (3)$$

where Q_0 is a normalization constant, α is the spectral index, E_c is the characteristic cutoff energy of electrons, β describes the sharpness of the cutoff, τ_0 is the time scale that the spindown luminosity of the pulsar starts to decay. The parameter τ_0 is difficult to be determined observationally, and we assume a nominal value of 10^4 yr in this work.

The propagation equation (1) can be solved analytically using the Green's function method with respect to variables \mathbf{r} and t (i.e., δ -function type injection for space and time), for an arbitrary injection spectrum [21]. Convolving the Green's function with the injection time profile, one can obtain the electron distribution at give time and position.

¹The magnetic field affects the relative weights between the synchrotron cooling rate and the ICS cooling rate. A weaker magnetic field would result in more significant impacts on the halo morphologies due to the Klein-Nishina effect and vice versa.

The photon emissivity due to the ICS is then given by

$$w_{\text{ICS}}(t, E_\gamma, \mathbf{r}) = \int_0^\infty d\epsilon n(\epsilon) \int_{E_{\text{min}}}^\infty dE_e N(t, E_e, \mathbf{r}) F(\epsilon, E_e, E_\gamma), \quad (4)$$

where $n(\epsilon)$ is the number density of background photons with energy ϵ , $N(t, E_e, \mathbf{r})$ is the electron density obtained via solving the propagation equation, and $F(\epsilon, E_e, E_\gamma)$ is the γ -ray yield function of the ICS according to the Klein-Nishina cross section. Integrating w_{ICS} along the line of sight, one can obtain the γ -ray surface brightness for specific energy E_γ .

3. Results

We take the Geminga pulsar halo as an example for the discussion. The distance of Geminga pulsar is adopted as $d_{\text{psr}} = 250 \text{ pc}$, and the age is $\tau_{\text{psr}} = 3.4 \times 10^5 \text{ yr}$ [22]. The diffusion coefficient is parameterized as a power-law of electron energy, $D(E_e) = D_0 (E_e/100 \text{ TeV})^\delta$. As a benchmark, $D_0 = 10^{27} \text{ cm}^2 \text{ s}^{-1}$ is assumed, which is several times smaller than that inferred by HAWC observations [12]. A smaller value of the diffusion coefficient is to avoid the complexity of the superluminal propagation at very small scales [23, 24], and does not loses generality of this work.

Figure 1 illustrates the influence of δ on the evolution of the γ -ray morphology with energy. The electron injection spectrum is assumed to be a power-law function with index $\alpha = 2.5$. Two values of δ , 0 and 1 are studied. Dashed lines in this plot correspond to $\delta = 0$, which show a clear contraction of the γ -ray extension with increasing energy. In this case, the energy loss rate of electrons increases with energy, but the diffusion coefficient keeps a constant, hence the characteristic diffusion distance $r_d \sim 2\sqrt{D(E_e)\tau(E_e)}$ becomes smaller when energy is higher. For $\delta = 1$, on the other hand, the characteristic diffusion length keeps almost unchanged, and the source extensions are similar at different energies as shown by solid lines. The extension at 100 TeV is slightly more extended than those at lower energies, due to that the ICS cooling rate becomes smaller and deviates from E_e^{-1} thanks to the Klein-Nishina effect.

Figure 2 shows the impact on the γ -ray morphologies from different injection spectra of electrons, for $\delta = 1$. Panel (a) shows the one-dimensional surface brightness distributions for power-law injection spectra with indices $\alpha = 1.5$ (solid lines) and $\alpha = 2.5$ (dashed lines). Panel (b) of Figure 2 illustrates the difference between the power-law injection spectrum (with $\alpha = 2.5$; dashed lines) and the power-law with super-exponential cutoff spectrum ($\alpha = 1.5$, $E_c = 100 \text{ TeV}$, $\beta = 2$; solid lines). To quantify the evolution of source extension, we fit the one-dimensional surface brightness distribution with the following profile [12]

$$f(\theta) \propto \frac{1}{\theta_d(\theta + 0.06\theta_d)} \cdot \exp[-(\theta/\theta_d)^2], \quad (5)$$

where $\theta_d = r_d/d_{\text{psr}}$ is the characteristic diffusion angle, and θ is the angular distance from the central pulsar. We assume 10% relative errors of the surface brightness profiles for each angular

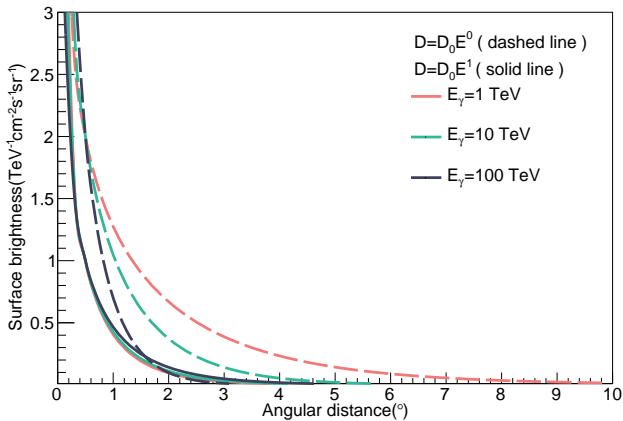


Figure 1: Surface brightness distributions of γ rays at different energies for $\delta = 1$ (solid lines) and $\delta = 0$ (dashed lines). The electron injection spectrum is a power-law form with spectral index $\alpha = 2.5$.

bin and adopt a minimum χ^2 method to do the fit. The evolution of θ_d for the three injection spectra are shown in panel (c). We can see that θ_d shows an increase trend when the energy increases for power-law injection, but shows a clear decrease trend for the spectrum with cutoff. It can also be noted that for $\alpha = 1.5$, the γ -ray profiles are typically more extended than the case of $\alpha = 2.5$. All these results show that the high-energy electron spectrum plays an important role in shaping the γ -ray morphologies.

To better understand these results, we scrutinize the distributions of electrons at different energies in detail. Figure 3 show the radial profiles of electron density as a function of distance from the pulsar, for different post-propagation energies and injection spectra. To eliminate the Klein-Nishina effect of the ICS, we test the case with synchrotron cooling only for a power-law injection, as shown by the solid lines. The results show that the spatial distributions of electrons with different energies are identical, just as expected for a cooling rate of E_e^{-1} and $\delta = 1$. However, when the ICS cooling is included (short-dashed lines), the cooling of higher energy electrons is smaller than E_e^{-1} , leading to more extended distributions of electrons with higher energies. As a result, the γ -ray morphology would also become more extended at higher energies, as shown in Figure 2. This also explains the morphology for harder spectrum ($\alpha = 1.5$) is more extended than that for softer spectrum ($\alpha = 2.5$), since there are more high-energy electrons for a harder spectrum. When there is cutoff of the injection spectrum, we in turn observe that higher energy electrons are less extended than low energy ones (long-dashed lines). In this case there are not many electrons at the source with energy high enough to cool down to given energy (e.g., $E_e = 300$ TeV). This could also be understood as that, under the continuous injection scenario, the current electron density is the time integral of the previously injected electron with higher energies. The decrease of high-energy electron flux for the cutoff spectrum is equivalent to a shorter effective integration time. The increase of the

diffusion coefficient with energy ($\sim E_e^1$) does not compensate the decrease in time, resulting in a decrease in θ_d . Therefore, we would observe a shrink of the γ -ray morphology with increasing energy if the source spectrum has a cutoff.

Finally, we show in Figure 4 the energy distribution of electrons which produce γ -rays with fixed energy E_γ , for different injection spectra. Due to the wide energy distributions of the ISRF and the ICS cross section, the electron energy distribution to give fixed E_γ is quite wide. For power-law injections, a harder spectrum corresponds to a longer high-energy tail of the electron energy distribution, which explains the larger extension of the γ -ray morphology as we discussed in above. The γ -ray morphologies from 1 TeV to 10 TeV evolve slowly with energy (see panel (c) of Figure 2), because the energies of electrons producing those γ rays are mainly below 100 TeV, and the Klein-Nishina effect of the cooling is not evident. However, from 10 TeV to 100 TeV, the Klein-Nishina effect becomes important, and the γ -ray extensions become significantly larger. For the injection spectrum with a curved shape, we can see that electron energy distributions are more concentrated than the power-law injection cases. Even if we observe the same morphology evolution of γ rays, the inferred energy-dependent diffusion properties are different for different injection spectra.

4. Conclusion and Discussion

Pulsar halos are formed by high-energy electrons and positrons injected from the associated pulsar wind nebulae via the ICS off the background photons [25, 26, 27, 28]. The γ -ray morphologies of pulsar halos are very important in revealing the particle propagation in the ISM around pulsars. It has been expected that the extension of the halo is proportional to the characteristic diffusion length scale, $\theta_d \propto r_d \propto 2\sqrt{D(E_e)\tau(E_e)}$. However, this expectation is over-simplified. In reality, the Klein-Nishina effect of the ICS cooling and the deviation of source injection spectrum from a power-law distribution affect the electron propagation and final distribution. As a consequence, the γ -ray morphology evolution also depends on the injection electron spectrum.

This study investigates the impacts of the electron injection spectrum on the γ -ray morphology evolution of pulsar halos. For simplicity, we take the energy-dependent slope of the diffusion coefficient $\delta = 1$ as a benchmark for discussion. Given the E_e^{-1} energy loss rate of electrons due to synchrotron and ICS cooling, this diffusion coefficient predicts energy-independent γ -ray morphologies. It has been shown that at relatively low energies (e.g., E_γ is smaller than tens of TeV), power-law injection spectrum indeed gives energy-independent source morphologies as expected. However, if E_γ is as high as tens of TeV, even power-law injection spectrum results in an evolution of the source extension. This is because the Klein-Nishina effect of the ICS leads to a less efficient cooling effect than the E_e^{-1} form. For power-law with super-exponential cutoff spectrum, a clear source contraction with increasing energy is given. We point out that such a contraction is due to that there are not enough high-energy electrons can contribute to those high-energy photons because of the spectral cutoff. It is thus necessary to take

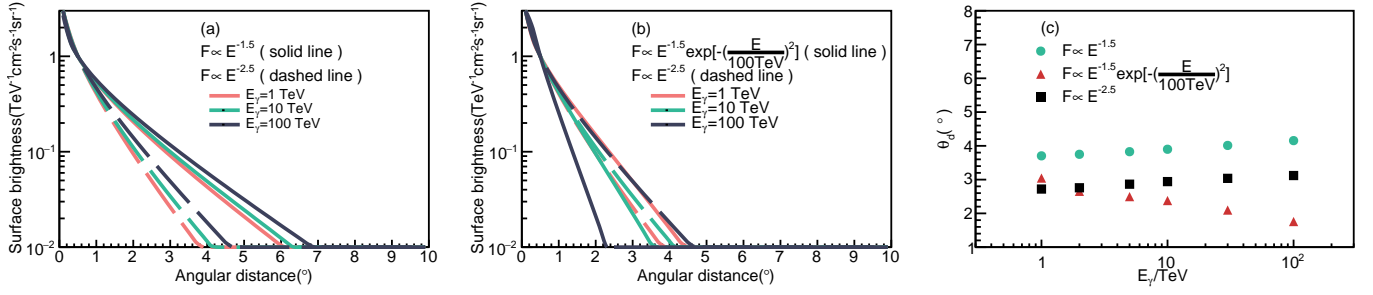


Figure 2: Impact on the γ -ray morphologies from different electron injection spectra. The energy-dependent slope of the diffusion coefficient is assumed to be $\delta = 1$. Panel (a): comparison of one-dimensional surface brightness distributions between power-law injection spectra with indices $\alpha = 1.5$ (solid lines) and $\alpha = 2.5$ (dashed lines). Panel (b): comparison of one-dimensional surface brightness distributions between power-law injection spectrum with index $\alpha = 2.5$ (dashed lines) and power-law with super-exponential cutoff spectrum $E_e^{-1.5} \exp[-(E_e/100 \text{ TeV})^2]$. Panel (c): variation of the diffusion angle θ_d with γ -ray energy for different injection spectra.

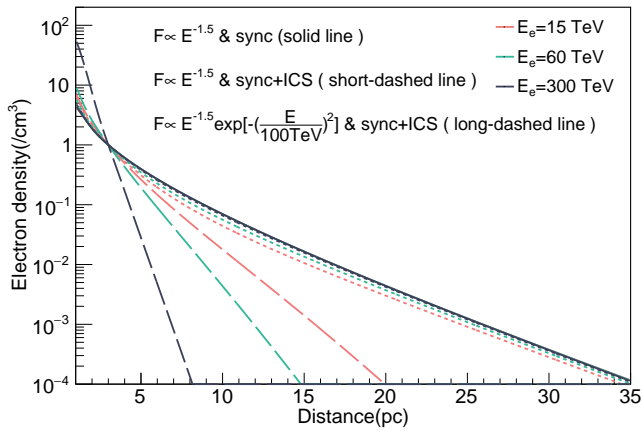


Figure 3: Impact on the electron morphologies with respect energy loss rate and injection spectra. The energy-dependent slope of the diffusion coefficient is assumed to be $\delta = 1$. All curves are normalized at 3 pc. In case of only synchrotron cooling, the radial profiles of electrons of different energies overlap with each other.

into account the injection spectrum shape when studying the energy-dependence of the diffusion coefficient using the UHE γ -ray observations.

Acknowledgments

This work is supported by the National Natural Science Foundation of China (No. 12220101003), the Project for Young Scientists in Basic Research of Chinese Academy of Sciences (No. YSBR-061), and the Jiangsu Provincial Excellent Post-doctoral Program with grant number 2022ZB472.

References

[1] V. S. Berezhinskii, S. V. Bulanov, V. A. Dogiel, and V. S. Ptuskin. *Astrophysics of cosmic rays*. Amsterdam: North-Holland, 1990, edited by Ginzburg, V.L., 1990.

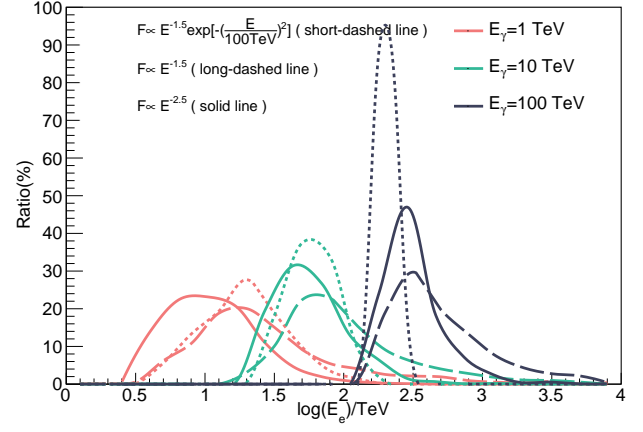


Figure 4: The fraction distribution of injection electron energies that produce γ rays with fixed energy E_γ .

[2] Andrew W. Strong, Igor V. Moskalenko, and Vladimir S. Ptuskin. Cosmic-Ray Propagation and Interactions in the Galaxy. *Annual Review of Nuclear and Particle Science*, 57(1):285–327, November 2007.

[3] Q. Yuan, S.-J. Lin, K. Fang, and X.-J. Bi. Propagation of cosmic rays in the AMS-02 era. *Phys. Rev. D*, 95(08):083007, April 2017.

[4] Q. Yuan. Implications on cosmic ray injection and propagation parameters from Voyager/ACE/AMS-02 nucleus data. *Science China Physics, Mechanics, and Astronomy*, 62:49511, April 2019.

[5] M. Aguilar, L. Ali Cavazonza, G. Ambrosi, L. Arruda, N. Attig, F. Barao, L. Barrin, A. Bartoloni, S. Başğömez-du Pree, J. Bates, and et al. The Alpha Magnetic Spectrometer (AMS) on the international space station: Part II - Results from the first seven years. *Phys. Rept.*, 894:1–116, February 2021.

[6] F. Alemanno, Q. An, P. Azzarello, F. Carla Tiziana Barbato, P. Bernardini, X. J. Bi, M. S. Cai, E. Casilli, E. Catanzani, J. Chang, et al. Detection of spectral hardenings in cosmic-ray boron-to-carbon and boron-to-oxygen flux ratios with DAMPE. *Science Bulletin*, 67(21):2162–2166, November 2022.

[7] Peng-Xiong Ma, Zhi-Hui Xu, Qiang Yuan, Xiao-Jun Bi, Yi-Zhong Fan, Igor V. Moskalenko, and Chuan Yue. Interpretations of the cosmic ray secondary-to-primary ratios measured by DAMPE. *Frontiers of Physics*, 18(4):44301, August 2023.

[8] N. Tomassetti. Origin of the Cosmic-Ray Spectral Hardening. *Astrophys. J. Lett.*, 752:L13, June 2012.

[9] C. Evoli, D. Gaggero, D. Grasso, and L. Maccione. Common Solution

- to the Cosmic Ray Anisotropy and Gradient Problems. *Phys. Rev. Lett.*, 108(21):211102, May 2012.
- [10] Y.-Q. Guo, Z. Tian, and C. Jin. Spatial-dependent Propagation of Cosmic Rays Results in the Spectrum of Proton, Ratios of P/P, and B/C, and Anisotropy of Nuclei. *Astrophys. J.*, 819:54, March 2016.
- [11] Y.-Q. Guo and Q. Yuan. Understanding the spectral hardenings and radial distribution of Galactic cosmic rays and Fermi diffuse γ rays with spatially-dependent propagation. *Phys. Rev. D*, 97(6):063008, March 2018.
- [12] A. U. Abeysekara, A. Albert, R. Alfaro, C. Alvarez, J. D. Álvarez, R. Arceo, J. C. Arteaga-Velázquez, D. Avila Rojas, H. A. Ayala Solares, A. S. Barber, and et al. Extended gamma-ray sources around pulsars constrain the origin of the positron flux at Earth. *Science*, 358:911–914, November 2017.
- [13] F. Aharonian, Q. An, Axikegu, L. X. Bai, Y. X. Bai, Y. W. Bao, D. Bastieri, X. J. Bi, Y. J. Bi, H. Cai, and et al. Extended Very-High-Energy Gamma-Ray Emission Surrounding PSR J 0622 +3749 Observed by LHAASO-KM2A. *Phys. Rev. Lett.*, 126(24):241103, June 2021.
- [14] K. Fang, X.-J. Bi, P.-F. Yin, and Q. Yuan. Two-zone Diffusion of Electrons and Positrons from Geminga Explains the Positron Anomaly. *Astrophys. J.*, 863:30, August 2018.
- [15] Stefano Profumo, Javier Reynoso-Cordova, Nicholas Kaaz, and Maya Silverman. Lessons from HAWC pulsar wind nebulae observations: The diffusion constant is not a constant; pulsars remain the likeliest sources of the anomalous positron fraction; cosmic rays are trapped for long periods of time in pockets of inefficient diffusion. *Phys. Rev. D*, 97(12):123008, June 2018.
- [16] Dan Hooper and Tim Linden. Measuring the local diffusion coefficient with H.E.S.S. observations of very high-energy electrons. *Phys. Rev. D*, 98(8):083009, October 2018.
- [17] Wei Liu, Yi-Qing Guo, and Qiang Yuan. Indication of nearby source signatures of cosmic rays from energy spectra and anisotropies. *J. Cosmol. Astropart. Phys.*, 10(10):010, Oct 2019.
- [18] Kun Fang, Xiao-Jun Bi, and Peng-Fei Yin. DAMPE Proton Spectrum Indicates a Slow-diffusion Zone in the nearby ISM. *Astrophys. J.*, 903(1):69, November 2020.
- [19] Kun Fang and Xiao-Jun Bi. Interpretation of the puzzling gamma-ray spectrum of the Geminga halo. *Phys. Rev. D*, 105(10):103007, May 2022.
- [20] Kun Fang, Xiao-Jun Bi, Su-Jie Lin, and Qiang Yuan. Klein-Nishina Effect and the Cosmic Ray Electron Spectrum. *Chinese Physics Letters*, 38(3):039801, March 2021.
- [21] A. M. Atayan, F. A. Aharonian, and H. J. Völk. Electrons and positrons in the galactic cosmic rays. *Phys. Rev. D*, 52:3265–3275, September 1995.
- [22] R. N. Manchester, G. B. Hobbs, A. Teoh, and M. Hobbs. The Australia Telescope National Facility Pulsar Catalogue. *Astron. J.*, 129:1993–2006, April 2005.
- [23] S. Recchia, M. Di Mauro, F. A. Aharonian, L. Orusa, F. Donato, S. Gabici, and S. Manconi. Do the Geminga, Monogem and PSR J0622+3749 γ -ray halos imply slow diffusion around pulsars? *Phys. Rev. D*, 104(12):123017, December 2021.
- [24] Li-Zhuo Bao, Kun Fang, Xiao-Jun Bi, and Sheng-Hao Wang. Slow Diffusion is Necessary to Explain the γ -Ray Pulsar Halos. *Astrophys. J.*, 936(2):183, September 2022.
- [25] Felix A. Aharonian. *Very high energy cosmic gamma radiation : a crucial window on the extreme Universe*. World Scientific Publishing, 2004.
- [26] G. Giacinti, A. M. W. Mitchell, R. López-Coto, V. Joshi, R. D. Parsons, and J. A. Hinton. Halo fraction in TeV-bright pulsar wind nebulae. *Astron. Astrophys.*, 636:A113, April 2020.
- [27] Kun Fang. Gamma-ray pulsar halos in the Galaxy. *Frontiers in Astronomy and Space Sciences*, 9:1022100, October 2022.
- [28] Ruo-Yu Liu. The physics of pulsar halos: Research progress and prospect. *International Journal of Modern Physics A*, 37(22):2230011, August 2022.